AE 3610, Lab #04

Sonic Adventure 2

By: **Madeleine Graham**

Group A11

Spring Semester 2023

Introduction

Supersonic Wind Tunnels make use of a converging-diverging nozzle to increase air flow to supersonic speeds. When air contracts at subsonic speeds through a converging nozzle, it speeds up isentropically, and reaches a limit, or "choke" point at Mach = 1. If the area of the nozzle is at a minimum and diverges again after converging and airflow is at a choked condition, the airflow will increase past Mach = 1. In a supersonic wind tunnel like the one used in this experiment, the speed of the wind tunnel is achieved through the geometry of the nozzle as well as application of a significant amount of pressure. Running the wind tunnel takes a large amount of power for a relatively short amount of time. However, understanding how objects behave in these conditions can help engineers optimize design for a multitude of purposes, including but not limited to: supersonic aircraft, missiles, rockets, and extra-planetary craft.

Data Results

Raw Data

Wind Tunnel Characterization

In order to find the Mach number at each station, the team ran the wind tunnel with no specimen in the test section and ran the Versatile Data Acquisition System (VDAS), which measured the gauge pressure and the pressure ratios (P0/P) at 25 stations along the length of the converging nozzle and test section. Table I, column 2 shows the raw data for P0/P acquired by the pressure taps at each station. This particular data was chosen from the samples VDAS recorded because all pressure tapping stations were stable, showing the same P0/P for at least two readings prior and two readings after the sample. This means that the sample I chose was during a time when the wind tunnel was at its most stable output.

Schlieren Images

The Schlieren imaging technique uses optics principles to be able to clearly visualize shock waves and to some extent, expansion waves. The supersonic wind tunnel was fitted with a halogen light, which shone first into a condenser lens, then a slit, then a mirror, then two lenses on either side of the clear windows of the test section. From there the silhouetted image of the test specimen and flow reflected off a mirror and got enhanced by going through a "Schlieren edge," which removed the light's intensity. Then the image was expanded and focused by another lens in order to project onto a screen. That screen was recorded by a camcorder which was connected via HDMI to an RGB monitor. Figures 3, 4, 5, and 6 are cell phone images taken of that RGB monitor during testing of a 10-degree wedge specimen with an angle of attack of 0, 2.5, 5, and 10 degrees respectively.

Ten-Degree Wedge Two-Pressure Tappings

In addition to the pressure taps present along the converging/diverging nozzle, there were two pressure taps on the ten-degree wedge specimen itself. The data recorded by the pressure taps was gauge pressure, which I used to calculate the static pressure values presented in Table III (see Data Reduction section below). Pressure ratio for pressure taps at stations 1-27 with the wedge specimen at three different angles of attack are presented in raw form in Table III.

Reduced Data

Wind Tunnel Characterization

Table I, column 3 displays the static pressure for each station. Static pressure was calculated by taking the gauge pressure measured by the VDAS and adding it to the atmospheric data also measured by the VDAS.

(Eq1) $$p_{static} = p_{gauge} + p_{atmospheric}$$

(Eq2) $$\frac{P}{P_0} = \left(1 + \frac{k-1}{2} M^2\right)^{\frac{-k}{k-1}}$$

(Eq3) $$\frac{A}{A^*} = \left(\frac{k+1}{2}\right)^{\frac{-k+1}{2(k-1)}} \left[\frac{\left(1+\frac{k-1}{2}M^2\right)^{\frac{k+1}{2(k-1)}}}{M}\right]$$

Mach number for each station is displayed in Table I. Because there are no shocks and heat added or removed from the system and friction effects can be ignored, I was able to calculate the Mach number by rearranging Eq2, which is a derived isentropic flow relation.

Similarly, I was able to find the area ratio between station areas and the area of the throat from the isentropic flow relation equation 3.

Figure 1 displays the relationship between Mach number found in Table I and distance along the converging section and test section of the wind tunnel and Figure 2 displays the relationship between area ratio found in Table I and distance. The pressure tap distance from the start of the converging section of the nozzle and the distance between each pressure tap were given.

10-Degree Double Wedge Experiment

Table II displays values oblique shock angle for each angle of attack, which I was able to calculate using an online protractor tool. I calculated the angle between the specimen's chord and the visible shock angle on the upper part of the specimen, then subtracted the angle of attack to get the shock angle. Column 3 in table II is the wedge angle, which I calculated by subtracting the angle of attack from the half-angle of the wedge specimen (5 degrees for all cases). The expansion fan angle is 10 degrees for all cases, because that is the angle which the freestream is allowed to expand at supersonic speed. To calculate the Mach number after the oblique shock, I used the relation in Eq 4 to solve for M_1:

(Eq 4) $$M_1^2 \sin^2(s-a) = \frac{(k-1)M_0^2 \sin^2 s+2}{2kM^2 \sin^2 s-(k-1)}$$

Where M_1 is the Mach number after the shock, s is the shock angle, a is the wedge angle, k is the specific heat ratio 1.4, and M_0 is the Mach number at station 18.

To solve for the Mach number after the expansion fan (M_2), I used Prandtl-Meyer tables (see Figure 7) and interpolated values by taking M_1, searching for the angle ν_0 associated with it, then adding the expansion fan angle to find ν_1. (Eq 5)

(Eq 5) $$\nu_1 = \nu_0 + \delta$$

Where δ is the expansion fan angle. After calculating ν_1, I used Excel's linear interpolation formula FORECAST.LINEAR() and the Prandtl-Meyer tables to calculate the corresponding Mach number.

During the Data Reduction process I also found Stagnation Pressures for Mach numbers directly before and after the oblique shock through the relation in Equation 6:

(Eq 6) $$\frac{P_{01}}{P_0} = \left[\frac{(k+1)M^2 \sin^2 s}{(k-1)M^2 \sin^2 s+2}\right]^{\frac{k}{k-1}} \left[\frac{(k+1)}{2kM^2 \sin^2 s-(k-1)}\right]^{\frac{1}{k-1}}$$

However, I found that the theoretical formulae for calculating Mach number after the expansion fan was analytically impossible to solve, and difficult for MATLAB or Excel to solve. I decided to use the table method, but given more time, I would have used numerical methods to solve Equations 7 and 8.

(Eq 7) $$\nu_0 = \sqrt{\frac{\gamma+1}{\gamma-1}}\ \tan^{-1}\sqrt{\frac{\gamma-1}{\gamma+1}\left(M_0^2-1\right)}\ -\ \tan^{-1}\sqrt{\left(M_0^2-1\right)}$$

(Eq 8) $$\nu_1 = \sqrt{\frac{\gamma+1}{\gamma-1}}\tan^{-1}\sqrt{\frac{\gamma-1}{\gamma+1}(M_1^2-1)} - \tan^{-1}\sqrt{(M_1^2-1)}$$

Discussion

Supplement Questions

1. Assume a pitot-static probe was inserted in the test section flow. Calculate the Po and measured and compare with that before the nozzle. Why do these compare the way they do?

If a pitot-static probe were entered into the test section, there would be a bow shock. So the pressure that the pitot-static probe would measure would be the pressures you'd find after a normal shock at a certain Mach number. Let's say that the pitot-static probe was inserted into the test section directly after Station 18, where the Mach number was measured to be around M_0 = 1.67. After the shock, the static pressure would relate to the static pressure prior to the shock via the following equations:

(Eq 9) $$\frac{P_{s1}}{P_{s0}} = \frac{2kM^2-(k-1)}{k+1}$$

(Eq 10) $$\frac{P_{01}}{P_0} = \left[\frac{(k+1)M^2}{(k-1)M^2+2}\right]^{\frac{k}{k-1}}\left[\frac{(k+1)}{2kM^2-(k-1)}\right]^{\frac{1}{k-1}}$$

If the total pressure before the shock P_0 is 1016.072 mbar (see Table I at station 18) and Mach is 1.67, then total pressure after the shock P_{01} is around 894 mbar. These differ because a normal shock causes severe pressure losses.

2. What assumption did you make to estimate Po in front of the nozzle? Discuss briefly.

I made the assumption that the inlet for the pitot-static probe was directly facing the stream such that I was able to use a normal shock relation and not need to account for the curvature of the bow shock.

3. What would happen in front of the wedge in the test section if the angle of the wedge was sufficiently increased?

If the angle were increased more, then there would be a bow shock ahead of the wedge. If the angle of the wedge were increased to 90 degrees there may be a normal shock.

4. If the wind tunnel had a fixed diffuser, what would be its minimum area if the Mach# in the test section is 1.8?

Ideally, the diffuser would have the same Area ratio A/A* as the converging-diverging nozzle section, which should be around 1.44 for Mach 1.8 (Eq 11).

(Eq 11)
$$\frac{A}{A^*} = \frac{1}{\mathrm{Ma}}\left[\left(\frac{2}{k+1}\right)\left(1+\frac{k-1}{2}\mathrm{Ma}^2\right)\right]^{0.5(k+1)/(k-1)}$$

However, in reality there is the starting problem: you can't just instantly have supersonic flow. Because the flow needs to start subsonic and increase to supersonic flow, there will be a shock in the test section. In order for the shock to live somewhere other than the test section where it can do less harm (result in less pressure loss), the area ratio of the diffuser has to be greater than A/A*. So the figure I gave of **1.44 is a minimum value**.

Additional Discussion

Pressure Tap 27

Pressure Tap 27 is clearly presenting some strange values. During the writing of this report, I

received information from the organization funding this experiment that the pressure tap 27 may have become pinched during the experiment. This is likely given that the pressure readings are very close to atmospheric pressure.

Schlieren images

The method of capturing the Schlieren images in this experiment could be vastly improved. One problem is that there is a camcorder trained on the screen. The camcorder is one level of obfuscation – how was the image on the video camera focused? Was it auto-focused? I did not see any specification on the camera in the lab manual, and certainly none of the members of our team knew how to calibrate such an outdated piece of equipment. Another layer, and this is probably the worst offender: the HDMI cable from the camcorder was attached to an RGB monitor. Figures 3 through 6 clearly display the telltale RGB pixels. To improve the visualizations in this experiment, instead of having a camcorder trained on the screen, just mount a cellphone and have the user take a picture or video directly of the screen. A cell phone camera would have captured a sharper image which is easier to analyze.

An oblique shock at 5 degrees angle of attack

Figure 5 shows our 10-degree wedge creating an oblique shock, even though the angle of attack was 5 degrees. Since the test specimen has a half-angle of 5 degrees, the airflow should have continued peacefully along the top of the wedge with no shock and an expansion fan in the middle. I suspect that the wind tunnel may not have been perfectly calibrated for the oblique shock to appear at this point in the experiment.

Odd Behavior in Figures 1 and 2

Figure 1 shows a steady increase in Mach number through the converging nozzle and to the test section, but after about 500 mm (Station 21 through 25), the behavior of the Mach number seems

odd. This is apparent in Figure 2 as well, which makes sense because the area ratio is calculated directly from the Mach values. I presume that the Mach number changes because there is some interference caused by the test section. Maybe this is due to a slight area change or the change in materials (the test section is glass and the enclosure seems to be metal). I would need to investigate the inside of the tunnel to get a better understanding of why the Mach number drops and oscillates at around Station 21.

Tables and Figures

Table I. Calculated Mach number and Area ratio for all stations 1 through 25 along the converging nozzle

Station #	P0/P	Static Pressure mbar	Mach #	A/A*
Station 1	1.120	907.000	0.405645	1.303462
Station 2	1.197	849.000	0.513417	1.116447
Station 3	1.218	834.000	0.538347	1.087472
Station 4	1.283	792.000	0.607438	1.026586
Station 5	1.382	735.000	0.695862	0.980785
Station 6	1.526	666.000	0.801096	0.960911
Station 7	1.725	589.000	0.918063	0.973053
THROAT*	**1.877**	545.000	**0.992509**	**0.996938**
Station 8	2.028	501.000	1.057983	1.027707
Station 9	2.515	404.000	1.227774	1.150082
Station 10	3.155	322.000	1.393881	1.334079
Station 11	4.016	253.000	1.561554	1.59625
Station 12	4.618	220.000	1.655688	1.783767
Station 13	4.704	216.000	1.667999	1.81072
Station 14	4.792	212.000	1.68034	1.838334
Station 15	4.838	210.000	1.686691	1.852782
Station 16	4.815	211.000	1.683524	1.845557
Station 17	4.885	208.000	1.693111	1.867552
Station 18	4.748	214.000	1.674201	1.824523
Station 19	5.030	202.000	1.712497	1.913172
Station 20	4.956	205.000	1.702681	1.88988
Station 21	3.299	308.000	1.425485	1.377151
Station 22	4.556	223.000	1.646652	1.764358

Station 23	3.375	301.000	1.441498	1.400042
Station 24	3.603	282.000	1.487063	1.469264
Station 25	3.024	336.000	1.363557	1.295299

NOTE: This particular row of data was used because it was within a zone of consistent values across the board for each station.

*Throat numbers from P0/P values interpolated between stations 7 and 8 because it is known there is an area minimum between the two stations. Calculations for throat included for idiot check

Table II. Values for Angle of attack, shock, edge, and expansion fan angle with calculated Mach number after the oblique shock and after the expansion fan for the 10-degree wedge.

Angle of Attack	Shock Angle	Wedge Angle	Expansion fan angle	Mach number after Oblique Shock	Mach number after Expansion Fan
deg	s, deg	a, deg	deg	M1	M2
0	40	5	10	1.62	1.97
2.5	41.5	2.5	10	1.44	1.78
5	42	0	10	1.34	1.68

Table III. Static Pressure and Pressure ratio with a 10-degree wedge specimen at stations 1-25, plus two pressure taps at the upper surface of the specimen, 26 and 27

Station #	Static Pressure mbar			Pressure Ratio (P/P0)		
	0 deg	2.5 deg	5 deg	0 deg	2.5 deg	5 deg
1	908	906	906	1.120	1.121	1.123
2	849	848	848	1.198	1.198	1.199
3	834	834	834	1.219	1.218	1.219
4	792	792	792	1.284	1.283	1.284
5	735	733	733	1.384	1.386	1.387
6	666	665	665	1.527	1.528	1.529
7	589	588	588	1.727	1.728	1.730
8	501	501	501	2.030	2.028	2.030
9	402	402	402	2.530	2.527	2.530
10	322	322	322	3.158	3.155	3.158
11	253	252	252	4.020	4.032	4.036
12	220	220	220	4.623	4.618	4.623

13	214	214	214	4.752	4.748	4.752
14	211	210	210	4.820	4.838	4.843
15	210	210	210	4.843	4.838	4.843
16	210	210	210	4.843	4.838	4.843
17	208	208	208	4.889	4.885	4.889
18	212	212	212	4.797	4.792	4.797
19	201	202	202	5.060	5.030	5.035
20	203	203	214	5.010	5.005	4.752
21	271	301	289	3.753	3.375	3.519
22	206	204	204	4.937	4.980	4.985
23	248	249	238	4.101	4.080	4.273
24	301	308	283	3.379	3.299	3.594
25	340	348	336	2.991	2.920	3.027
26	185	183	177	5.497	5.552	5.746
27	1012	1013	1013	1.005	1.003	1.004

Table IV. Pressure Ratios after oblique shock and expansion fan, with Mach numbers after oblique shock and expansion fan calculated from pressure ratios at angles of attack of 0, 2.5, and 5 degrees.

Angle of attack deg	Pressure Ratio After Oblique Shock (P/P0)	Pressure Ratio After Expansion fan (P/P0)	Mach Number After Oblique Shock M1	Mach Number after Expansion Fan M2
0	5.497	1.005	1.771	0.084
2.5	5.552	1.003	1.778	0.065
5	5.746	1.004	1.800	0.076

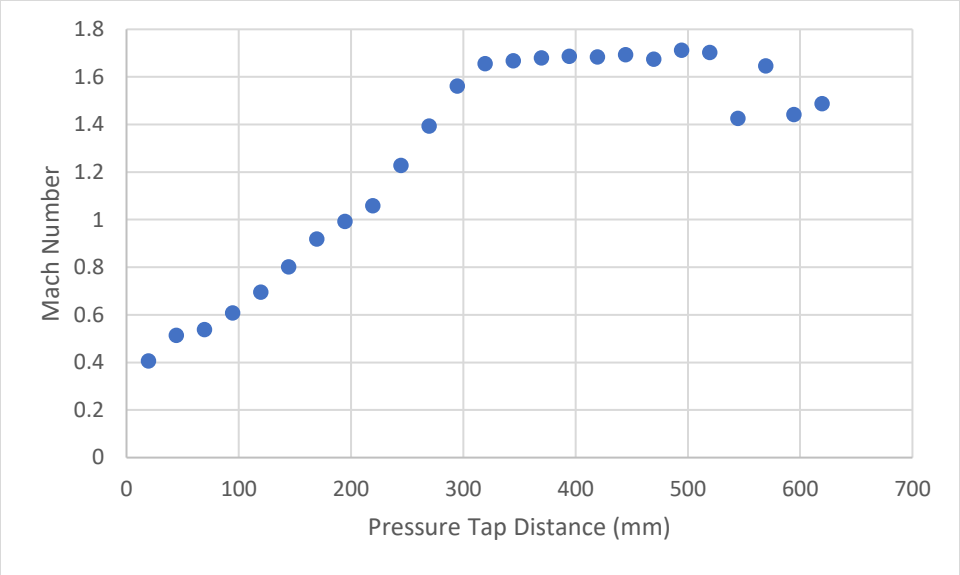

Figure 1. Mach number vs. Pressure Tap Distance from start of the converging nozzle to the end of the test section.

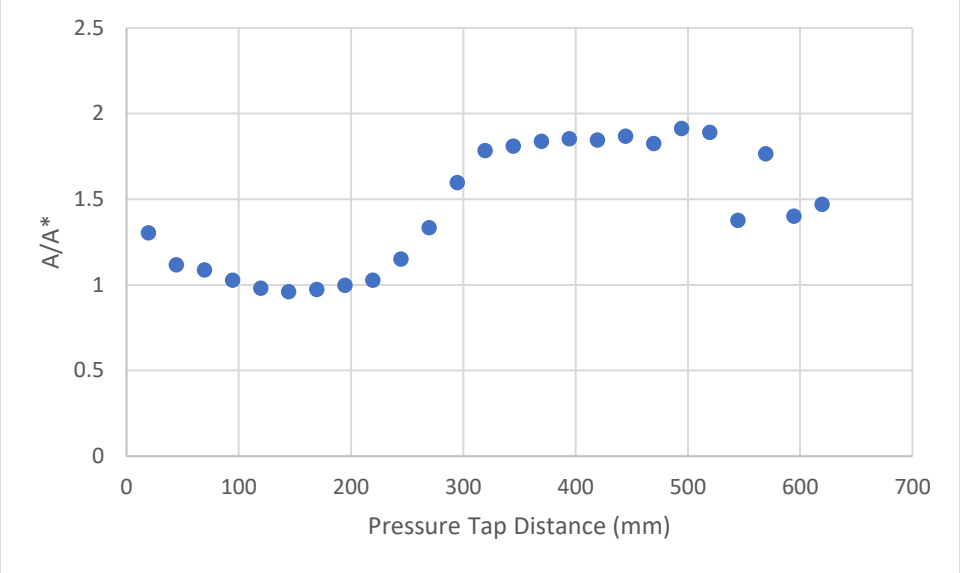

Figure 2. Area Ratio vs. Pressure Tap Distance from the start of the converging nozzle to the end of the test section.

Figure 3: A photo of the Schlieren visualization of the 10-degree wedge at 0 degrees. The image is flipped vertically to show the true top, rather than the upside-down Schlieren-reversed image.

Figure 4: A photo of the Schlieren visualization of the 10-degree wedge at 2.5 degrees counter-clockwise turn. The image is flipped vertically to show the true top, rather than the upside-down Schlieren-reversed image.

Figure 5: A photo of the Schlieren visualization of the 10-degree wedge at 5 degrees counter-clockwise turn. The image is flipped vertically to show the true top, rather than the upside-down Schlieren-reversed image.

Figure 6: A photo of the Schlieren visualization of the 10-degree wedge at 10 degrees counter-clockwise turn. The image is flipped vertically to show the true top, rather than the upside-down Schlieren-reversed image. There is no shock on the bottom of the specimen because the flow did

APPENDIX D

Prandtl Meyer Functions ($\gamma = 1.4$)

M	ν	μ	M	ν	μ
1.00	0	90.00	1.60	14.861	38.68
1.01	.04473	81.93	1.61	15.156	38.40
1.02	.1257	78.64	1.62	15.452	38.12
1.03	.2294	76.14	1.63	15.747	37.84
1.04	.3510	74.06	1.64	16.043	37.57
1.05	.4874	72.25	1.65	16.338	37.31
1.06	.6367	70.63	1.66	16.633	37.04
1.07	.7973	69.16	1.67	16.928	36.78
1.08	.9680	67.81	1.68	17.222	36.53
1.09	1.148	66.55	1.69	17.516	36.28

Figure 7: A snapshot of a table of Prandtl-Meyer Functions Tabulated (complete tables not included).

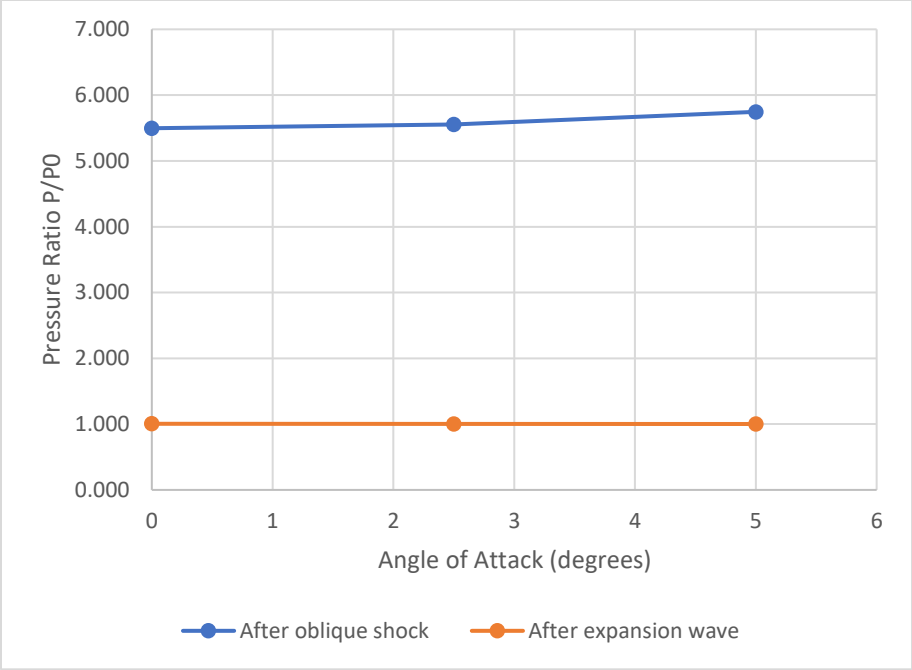

Figure 8: Trend of Pressure ratio after oblique shock and after expansion wave with respect to angle of attack.

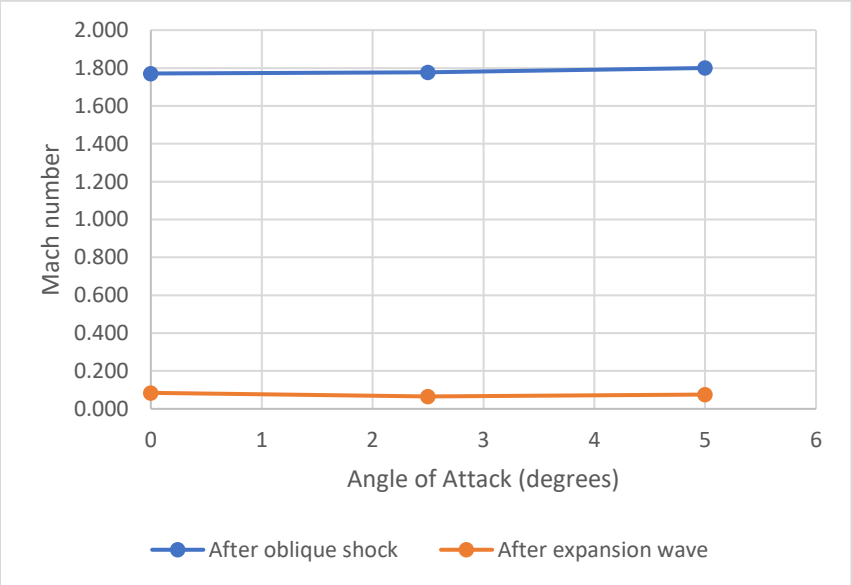

Figure 9: Trend of Mach number after oblique shock and after expansion wave with respect to angle of attack.

Figure 10: Sonic Adventure 2 for the Dreamcast has the same name as this report, but it's nowhere near as exciting. Sonic the Hedgehog does not even approach Mach 1 while "rolling around at the speed of sound."